ELSEVIER

International Journal of Heat and Fluid Flow 21 (2000) 535–541

International Journal of HEAT AND FLUID FLOW

www.elsevier.com/locate/ijhff

Scalar transport and mixing in turbulent stratified shear flow

Frank G. Jacobitz *

Department of Mechanical Engineering, University of California, Riverside, CA 92521-0425, USA

Abstract

In this study, the evolution of the velocity field and scalar concentration fields in stably stratified shear flow is studied using direct numerical simulations. Two cases with vertical mean shear and horizontal mean shear are compared. In both cases, the growth of the turbulent kinetic energy weakens as the Richardson number is increased. However, the horizontal shear case shows a stronger growth of the turbulent kinetic energy than the vertical shear case for a given Richardson number. The ordering of the velocity components was found to change from *streamwise* > *horizontal* > *vertical* in the vertical shear case to *streamwise* > *vertical* > *horizontal* in the horizontal shear case. The fluctuation level of a passive species variable with a vertical mean gradient was observed to be stronger in the horizontal shear case. The ratio of the vertical turbulent eddy diffusivity to the horizontal turbulent eddy diffusivity was found to be larger in the horizontal shear case.

Keywords: Geophysical turbulence; Shear flow; Density stratification; Anisotropy properties; Passive scalar mixing

1. Introduction

Shear and stratification are important features of turbulent flow in geophysical, environmental, and engineering applications. Nutrients, pollutants, or reactants present in these flows are transported and mixed by the turbulent motion. However, the turbulence evolution is influenced by the competing effects of shear and stratification. A review of geophysical turbulence can be found in Caldwell (1987) and in Caldwell and Moum (1995).

In this study, the prototypical example of stratified shear flow with uniform vertical stratification $S_\rho = \partial\overline{\varrho}/\partial x_3$ and uniform vertical shear $S_V = \partial\overline{U_1}/\partial x_3$ or uniform horizontal shear $S_H = \partial\overline{U_1}/\partial x_2$ is considered. In addition, two passive species variables C_i are introduced with uniform mean gradients in the vertical direction $H_3 = \partial\overline{C_3}/\partial x_3$ and in the horizontal direction $H_2 = \partial\overline{C_2}/\partial x_2$.

Previous work has been focused on the vertical shear case. Laboratory experiments have been performed by Rohr et al. (1988) in a salt-stratified water channel and by Piccirillo and Van Atta (1997) in a thermally stratified wind tunnel. Direct numerical simulations have been performed by Gerz et al. (1989), Holt et al. (1992), and Jacobitz et al. (1997). In these investigations, the gradient Richardson number $Ri = N^2/S^2$ was identified as the primary parameter in stratified shear flow. Here $N = (-gS_\rho/\rho_0)^{1/2}$ is the Brunt–Väisälä frequency, S the shear rate, g the gravity acceleration, and ρ_0 the ambient density. Note that S can refer to the vertical shear rate S_V was well as to the horizontal shear rate S_H. Passive species variables were included in the large eddy simulations by Kaltenbach et al. (1994). It was found that the turbulent mixing of these concentration fields is stronger in the horizontal direction than in the vertical direction.

Nonvertical shear flow has been studied only recently by Jacobitz and Sarkar (1998). It was found that the turbulent fluctuations as well as the vertical transport are stronger in the horizontal shear case. However, it was impossible to compare horizontal momentum and mass transfer in the horizontal shear simulations, since the mass transfer was always in the vertical direction. The introduction of concentration fields makes such a comparison possible in the present study.

A number of geophysical and environmental applications may have a significant amount of horizontal shear. Farmer et al. (1995) observed strong horizontal shear and mixing in Haro Strait and so did the numerical simulations by Foreman et al. (1993) of the same flow. Farmer et al. report horizontal shear as large as $S_H = 0.15\ s^{-1}$ at the frontal zone between the confluence of tidal waters with different densities from the Haro and Spieden Channels. The vertical shear can be estimated from the maximum current speed of 1 m s^{-1} and layer thickness of 50 m as $S_V = 0.02\ s^{-1}$. Lueck and Mudge (1997) found greatly increased dissipation rates in the vicinity of a shallow seamount. Although vertical shear is large in the vicinity of bottom topography, the horizontal shear component can be substantial due to the horizontal variability of the topographic features. Mixing near boundaries may be an important contributor to the overall budget of ocean mixing as proposed by Armi (1978) and thus reconcile the apparent order of magnitude larger vertical diffusivity inferred from global budgets by Munk (1966) with respect to that observed in the main thermocline (see for example, Gregg, 1987). If boundary mixing is indeed important, then flows with more

* Tel.: +1-909-787-2927; fax: +1-909-787-2899.
E-mail address: jacobitz@engr.ucr.edu (F.G. Jacobitz).

0142-727X/00/$ - see front matter
PII: S0142-727X(00)00042-4

Notation

C_i	total passive scalar
c_i	fluctuating passive scalar
g	gravity acceleration
H_2	horizontal mean gradient, $\partial\overline{C_2}/\partial x_2$
H_3	vertical mean gradient, $\partial\overline{C_3}/\partial x_3$
K	turbulent kinetic energy, $\overline{u_iu_i}/2$
K_ρ	potential energy, $-\overline{\rho\rho}g/(2\rho_0 S_\rho)$
N	Brunt–Väisälä frequency, $(-gS_\rho/\rho_0)^{1/2}$
Pr	Prandtl number, ν/α_ρ
p	fluctuating pressure
q	velocity magnitude, $(\overline{u_iu_i})^{1/2}$
Re_λ	Taylor microscale Reynolds number, $q\lambda/\nu$
Ri	Richardson number, N^2/S^2
S	horizontal or vertical shear rate
S_H	horizontal shear rate, $\partial\overline{U_1}/\partial x_2$
S_V	vertical shear rate, $\partial\overline{U_1}/\partial x_3$
S_ρ	vertical stratification rate, $\partial\overline{\varrho}/\partial x_3$
Sc	Schmidt number, ν/α
U_i	total velocity
u_i	fluctuating velocity
α	passive scalar diffusivity
α_ρ	density diffusivity
ϵ	dissipation rate, $\nu\overline{(\partial u_i/\partial x_k)(\partial u_k/\partial x_i)}$
λ	Taylor microscale, $(5\nu q^2/\epsilon)^{1/2}$
ν	kinematic viscosity
ϱ	total density
ρ	density fluctuation
ρ_0	ambient density

complex shear than the well-studied vertical shear case require systematic investigation.

In the next section, important definitions and equations are introduced. Then, the results of the simulations are presented. First, the evolution of the velocity field is summarized. Then, the evolution of the concentration fields is presented and compared to the velocity field. Finally, the turbulent mixing properties of the velocity and concentration fields are compared. The last section contains a summary of this work.

2. Equations

This study is based on the continuity equation of an incompressible fluid, the unsteady three-dimensional Navier–Stokes equation in the Boussinesq approximation, and transport equations for the density and concentration fields. In the following, x_1 refers to the streamwise direction, x_2 to the horizontal direction, and x_3 to the vertical direction. The total values of the velocity components U_i, the density ϱ, and the concentration fields C_i are decomposed into a mean part (denoted by an overbar) and a fluctuating part (denoted by a small character):

$$U_i = \overline{U}_i + u_i, \qquad \varrho = \overline{\varrho} + \rho, \qquad C_i = \overline{C}_i + c_i. \tag{1}$$

The mean parts have uniform gradients. In the vertical shear case $\overline{U_i} = S_V x_3 \delta_{i1}$ and in the horizontal shear case $\overline{U_i} = S_H x_2 \delta_{i1}$. Furthermore $\overline{\varrho} = \rho_0 + S_\rho x_3$ and $\overline{C}_\alpha = H_\alpha x_\alpha$. Summation is implied over repeated Arabic indices but not over Greek indices. Note, that indices are used to distinguish the components of the velocity field as well as the different concentration fields. While the components of the velocity field depend on each other through the nonlinear term in the Navier–Stokes equation, the different concentration fields are independent of each other and the index refers to the orientation of the mean concentration gradient.

Transport equations can be derived from the equations of motion (e.g. Lesieur, 1993):

$$\frac{\mathrm{d}}{\mathrm{d}t}\overline{u_1u_1} = -2S_V\overline{u_1u_3} - 2S_H\overline{u_1u_2} + \frac{2}{\rho_0}\overline{p\frac{\partial u_1}{\partial x_1}} - 2\nu\overline{\frac{\partial u_1}{\partial x_k}\frac{\partial u_1}{\partial x_k}}, \tag{2}$$

$$\frac{\mathrm{d}}{\mathrm{d}t}\overline{u_2u_2} = \frac{2}{\rho_0}\overline{p\frac{\partial u_2}{\partial x_2}} - 2\nu\overline{\frac{\partial u_2}{\partial x_k}\frac{\partial u_2}{\partial x_k}}, \tag{3}$$

$$\frac{\mathrm{d}}{\mathrm{d}t}\overline{u_3u_3} = -2\frac{g}{\rho_0}\overline{u_3\rho} + \frac{2}{\rho_0}\overline{p\frac{\partial u_3}{\partial x_3}} - 2\nu\overline{\frac{\partial u_3}{\partial x_k}\frac{\partial u_3}{\partial x_k}}, \tag{4}$$

$$\frac{\mathrm{d}}{\mathrm{d}t}\overline{u_1u_2} = -S_V\overline{u_2u_3} - S_H\overline{u_2u_2} + \frac{1}{\rho_0}\left(\overline{p\frac{\partial u_1}{\partial x_2}} + \overline{p\frac{\partial u_2}{\partial x_1}}\right) - 2\nu\overline{\frac{\partial u_1}{\partial x_k}\frac{\partial u_2}{\partial x_k}}, \tag{5}$$

$$\frac{\mathrm{d}}{\mathrm{d}t}\overline{u_1u_3} = -S_V\overline{u_3u_3} - S_H\overline{u_2u_3} - \frac{g}{\rho_0}\overline{u_1\rho} + \frac{1}{\rho_0}\left(\overline{p\frac{\partial u_1}{\partial x_3}} + \overline{p\frac{\partial u_3}{\partial x_1}}\right) - 2\nu\overline{\frac{\partial u_1}{\partial x_k}\frac{\partial u_3}{\partial x_k}}, \tag{6}$$

$$\frac{\mathrm{d}}{\mathrm{d}t}\overline{u_2u_3} = -\frac{g}{\rho_0}\overline{u_2\rho} + \frac{1}{\rho_0}\left(\overline{p\frac{\partial u_2}{\partial x_3}} + \overline{p\frac{\partial u_3}{\partial x_2}}\right) - 2\nu\overline{\frac{\partial u_2}{\partial x_k}\frac{\partial u_3}{\partial x_k}}, \tag{7}$$

$$\frac{\mathrm{d}}{\mathrm{d}t}\overline{c_2c_2} = -2H_2\overline{u_2c_2} - 2\alpha\overline{\frac{\partial c_2}{\partial x_k}\frac{\partial c_2}{\partial x_k}}, \tag{8}$$

$$\frac{\mathrm{d}}{\mathrm{d}t}\overline{c_3c_3} = -2H_3\overline{u_3c_3} - 2\alpha\overline{\frac{\partial c_3}{\partial x_k}\frac{\partial c_3}{\partial x_k}}, \tag{9}$$

$$\frac{\mathrm{d}}{\mathrm{d}t}\overline{u_2c_2} = -H_2\overline{u_2u_2} + \frac{1}{\rho_0}\overline{p\frac{\partial c_2}{\partial x_2}} - \frac{\nu}{\alpha}(\nu+\alpha)\overline{\frac{\partial c_2}{\partial x_k}\frac{\partial u_2}{\partial x_k}}, \tag{10}$$

$$\frac{\mathrm{d}}{\mathrm{d}t}\overline{u_3c_3} = -H_3\overline{u_3u_3} - \frac{g}{\rho_0}\overline{c_3\rho} + \frac{1}{\rho_0}\overline{p\frac{\partial c_3}{\partial x_3}} - \frac{\nu}{\alpha}(\nu+\alpha)\overline{\frac{\partial c_3}{\partial x_k}\frac{\partial u_3}{\partial x_k}}, \tag{11}$$

$$\frac{\mathrm{d}}{\mathrm{d}t}\overline{\rho\rho} = -2S_\rho\overline{u_3\rho} - 2\alpha_\rho\overline{\frac{\partial\rho}{\partial x_k}\frac{\partial\rho}{\partial x_k}}, \tag{12}$$

where ν is the viscosity of the velocity field, α the diffusivity of the concentration fields, and α_ρ the diffusivity of the density field. In these equations S_V is zero for the horizontal shear case and S_H is zero for the vertical shear case. A transport equations for the turbulent kinetic energy $K = \overline{u_iu_i}/2$ can be derived from Eqs. (2)–(4):

$$\frac{\mathrm{d}}{\mathrm{d}t}K = -S_V\overline{u_1u_3} - S_H\overline{u_1u_2} - \frac{g}{\rho_0}\overline{u_3\rho} - \nu\overline{\frac{\partial u_i}{\partial x_k}\frac{\partial u_i}{\partial x_k}}. \tag{13}$$

The potential energy $K_\rho = -\overline{\rho\rho}g/(2\rho_0 S_\rho)$ can be computed from the density fluctuations.

3. Results

In the following sections, the results from two series of simulations are presented. The first series has vertical shear and the second series has horizontal shear. Both series are

vertically stably stratified. In both series of simulations, the Richardson number is varied from $Ri = 0$ to $Ri = 0.5$. All simulations are initialized with an isotropic turbulence field without fluctuations in the density and concentration fields. The initial values of the Taylor microscale Reynolds number $Re_\lambda = q\lambda/\nu = 33.54$ and the shear number $SK/\epsilon = 2.0$ are fixed. Here $q = (\overline{u_i u_i})^{1/2}$ is the magnitude of the velocity, $\lambda = (5\nu q^2/\epsilon)^{1/2}$ is the Taylor microscale, and $\epsilon = \nu\overline{(\partial u_i/\partial x_k)(\partial u_i/\partial x_k)}$ is the dissipation rate. The Schmidt number $Sc = \nu/\alpha = 0.72$ and the Prandtl number $Pr = \nu/\alpha_\rho = 0.72$ are fixed.

3.1. Velocity field

In this section, the evolution of the velocity field is discussed. Fig. 1 shows the evolution of the turbulent kinetic energy K as a function of the Richardson number Ri. Initially, the turbulent kinetic energy decays due to the isotropic initial conditions. The further evolution depends on the value of the Richardson number and on the direction of shear. As the Richardson number is increased, the growth of the turbulent kinetic energy weakens for both the vertical and horizontal shear cases. In the vertical shear case, decay of K is found for Richardson numbers $Ri > 0.1$. It was shown by Jacobitz and Sarkar (1998) that $Ri > 1.0$ in required to observe decay of K in the horizontal shear case. Also, for a given Richardson number Ri, the horizontal shear case always shows stronger growth than the vertical shear case. This is due to a direct influence of gravity on the production term $-S_V\overline{u_1 u_3}$ in the vertical shear case (see Eq. (6)), but not on the production term $-S_H\overline{u_1 u_2}$ in the horizontal shear case (see Eq. (5)). Details on the evolution of the turbulent kinetic energy K can be found in Jacobitz and Sarkar (1998).

The evolution of the ratio of potential energy to turbulent kinetic energy K_ρ/K is shown in Fig. 2. In the vertical shear case, the ratio K_ρ/K reaches a constant value, indicating a similar evolution of turbulent kinetic and potential energy. In the horizontal shear case, this ratio tends to decrease in time. This decrease is due to a reduced production of potential energy in the horizontal shear case.

Fig. 3 shows the evolution of the square of the velocity components $u_1^2 = \overline{u_1 u_1}$, $u_2^2 = \overline{u_2 u_2}$, and $u_3^2 = \overline{u_3 u_3}$. The turbulent kinetic energy is unevenly distributed over the three components. The streamwise component u_1^2 is the largest component. This is due to turbulent production adding energy to the streamwise component (see Eq. (2)). The energy is then redistributed by the pressure–strain terms into the horizontal and vertical velocity components. Finally, the buoyancy flux converts vertical kinetic energy into potential energy (see Eq. (4)). This suggests an ordering $u_1^2 > u_2^2 > u_3^2$. This is indeed found for all Richardson numbers in the vertical shear case as shown in Fig. 4. However, the horizontal shear simulations show a different ordering $u_1^2 > u_3^2 > u_2^2$. In the horizontal shear case, the vertical component is larger than the horizontal component.

This can be explained with a different pressure–strain redistribution of turbulent kinetic energy from the streamwise velocity component into the horizontal and vertical velocity components. Fig. 5 shows the evolution of the ratio of the pressure–strain terms $-\Pi_{33}/\Pi_{11}$ and $-\Pi_{22}/\Pi_{11}$ for the vertical and horizontal shear cases. The dependence of the pressure–strain terms on the Richardson number Ri at nondimensional time $St = 10$ is shown in Fig. 6. Here, $\Pi_{11} = 2\overline{p\partial u_1/\partial x_1}/\rho_0$, $\Pi_{22} = 2\overline{p\partial u_2/\partial x_2}/\rho_0$, and $\Pi_{33} = 2\overline{p\partial u_3/\partial x_3}/\rho_0$. Note that $\Pi_{11} + \Pi_{22} + \Pi_{33} = 0$. Generally, the vertical velocity component receives more energy than the horizontal velocity component. However, in the horizontal shear case, that difference

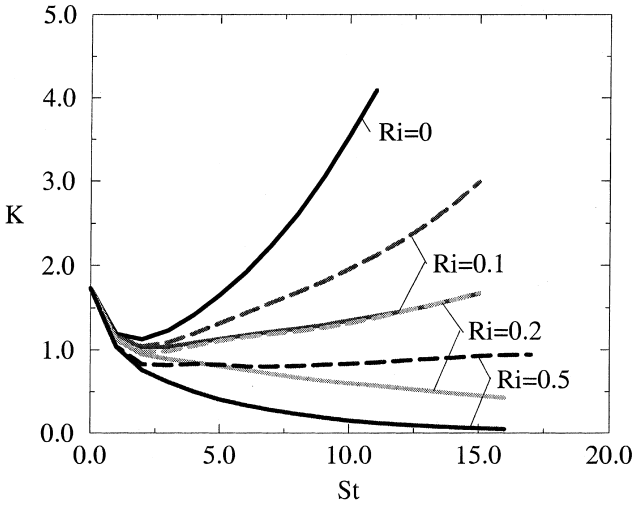

Fig. 1. Evolution of the turbulent kinetic energy K as a function of the Richardson number Ri for the vertical shear case (solid lines) and the horizontal shear case (dashed lines).

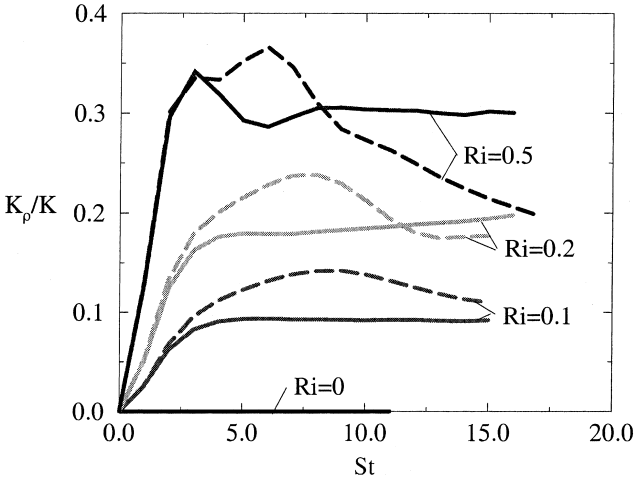

Fig. 2. Evolution of the ratio of potential energy to turbulent kinetic energy K_ρ/K as a function of the Richardson number Ri for the vertical shear case (solid lines) and the horizontal shear case (dashed lines).

is larger than in the vertical shear case. In the horizontal shear case, the pressure–strain redistribution is large enough to compensate for the loss of vertical kinetic energy due to the buoyancy flux. Therefore, the vertical velocity component u_3^2 contains more energy than the horizontal component u_2^2 in the horizontal shear case.

3.2. Concentration fields

In this section, the evolution of two scalar variables is discussed. The first scalar C_2 has a uniform mean gradient $H_2 = \partial\overline{C_2}/\partial x_2$ in the horizontal direction and the second scalar C_3 has a uniform mean gradient $H_3 = \partial\overline{C_3}/\partial x_3$ in the vertical direction.

Fig. 7 shows the evolution of the square of the fluctuating concentrations $c_3^2 = \overline{c_3 c_3}$ and $c_2^2 = \overline{c_2 c_2}$ for the vertical and horizontal shear cases with $Ri = 0.2$. In the vertical shear case, c_2^2 is much larger than c_3^2. This is consistent with the ordering of

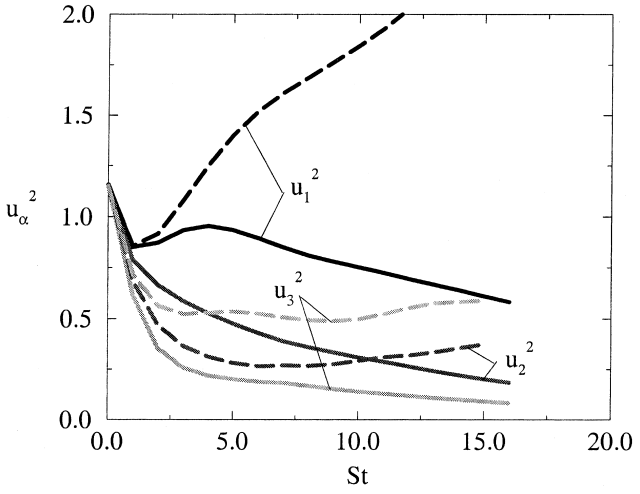

Fig. 3. Evolution of the square of the velocity components u_1^2, u_2^2, and u_3^2 for the vertical shear case (solid lines) and the horizontal shear case (dashed lines). The Richardson number is $Ri = 0.2$.

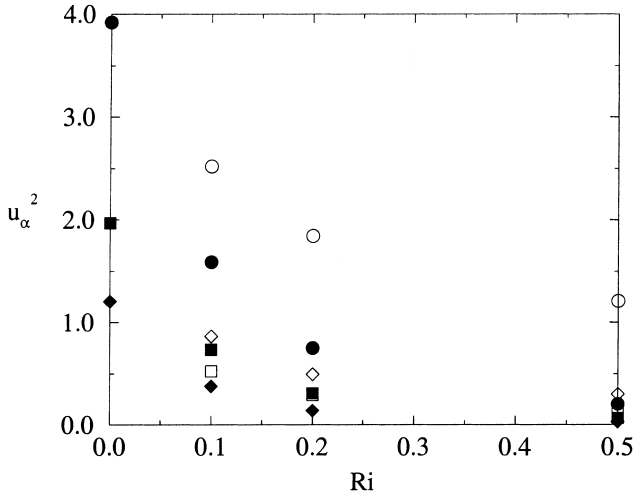

Fig. 4. Dependence of the square of the velocity components u_1^2, u_2^2, and u_3^2 on the Richardson number Ri for the vertical shear case (filled symbols) and the horizontal shear case (open symbols) at nondimensional time $St = 10$. Circles correspond to u_1^2, squares to u_2^2, and diamonds to u_3^2.

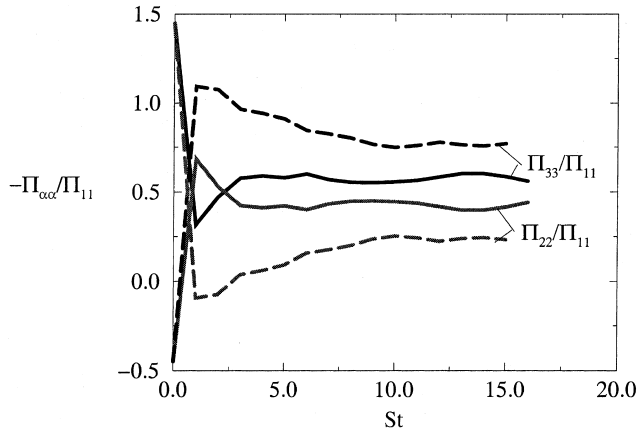

Fig. 5. Evolution of the pressure–strain ratio $-\Pi_{33}/\Pi_{11}$ and $-\Pi_{22}/\Pi_{11}$ for the vertical shear case (solid lines) and the horizontal shear case (dashed lines). The Richardson number is $Ri = 0.2$.

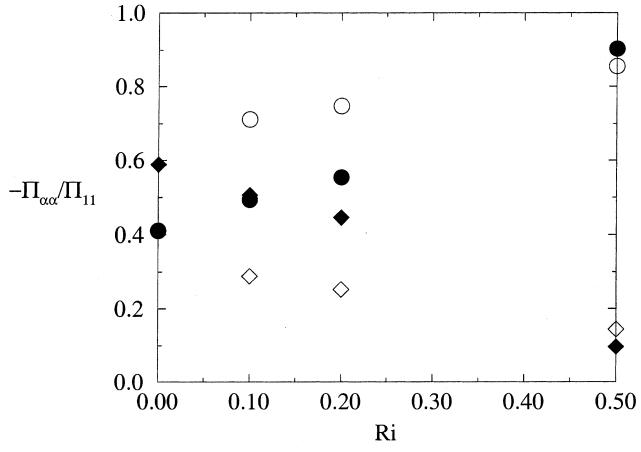

Fig. 6. Dependence of the pressure–strain ratio $-\Pi_{33}/\Pi_{11}$ and $-\Pi_{22}/\Pi_{11}$ on the Richardson number Ri for the vertical shear case (filled symbols) and the horizontal shear case (open symbols) at nondimensional time $St = 10$. Circles correspond to $-\Pi_{33}/\Pi_{11}$ and diamonds correspond to $-\Pi_{22}/\Pi_{11}$.

the square of the vertical and horizontal velocity components with $u_2^2 > u_3^2$. In the horizontal shear case, c_2^2 is only slightly larger than c_3^2. This is in contrast to the ordering of the square of the velocity components with $u_3^2 > u_2^2$. However, c_3^2 is strongly increased in the horizontal shear case compared to the vertical shear case.

Fig. 8 shows the dependence of the square of the fluctuating concentrations as a function of the Richardson number at nondimensional time $St = 10$. Only in the weakly stratified case with $Ri = 0.1$ is c_3^2 larger than c_2^2 in the horizontal shear case.

The difference in the ordering of velocity components and concentration fluctuations can be explained with a different production mechanism. The horizontal and vertical velocity components gain energy from a pressure–strain redistribution from the streamwise velocity component. However, the production terms $-2H_2\overline{u_2c_2}$ and $-2H_3\overline{u_3c_3}$ generate the fluctuations of the concentration fields (see Eqs. (8) and (9)). The vertical scalar production $-2H_3\overline{u_3c_3}$ is directly influenced by gravity (see Eq. (11)), but the horizontal scalar production $-2H_2\overline{u_2c_2}$ is not directly influenced by gravity (see Eq. (10)).

Fig. 9 shows the dependence of the correlation coefficients $R(u_\alpha c_\alpha) = \overline{u_\alpha c_\alpha}/(\overline{u_\alpha u_\alpha}\,\overline{c_\alpha c_\alpha})^{1/2}$ on the Richardson number Ri at nondimensional time $St = 10$. In the vertical shear case, the magnitude of $R(u_2c_2)$ increases as the Richardson number is increased, but the magnitude of $R(u_3c_3)$ decreases strongly and $R(u_3c_3)$ changes sign for the $Ri = 0.5$ case. In the horizontal shear case, the magnitude of $R(u_2c_2)$ remains almost constant and the magnitude of $R(u_3c_3)$ decreases slightly. This explains, first, the ordering of the concentration fluctuations in the vertical and horizontal shear cases and, second, the reduced difference between c_2^2 and c_3^2 observed in the horizontal shear case. Note that $R(u_3c_3)$ changes sign for large Richardson number, indicating a counter-gradient flux in the vertical shear case, but not in the horizontal shear case.

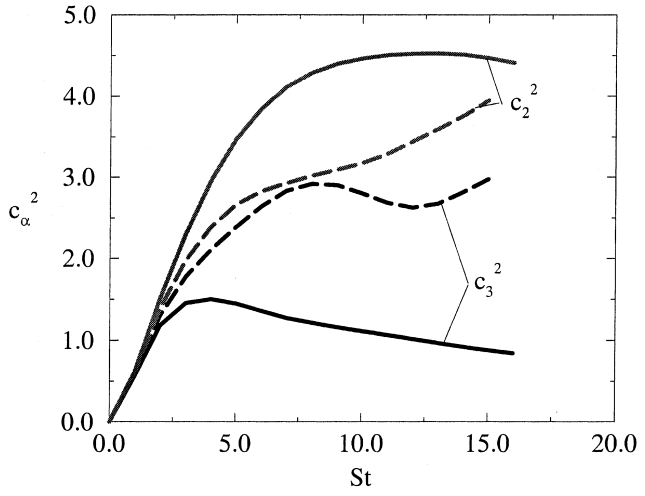

Fig. 7. Evolution of the square of the concentration fluctuations c_2^2 and c_3^2 for the vertical shear case (solid lines) and the horizontal shear case (dashed lines). The Richardson number is $Ri = 0.2$.

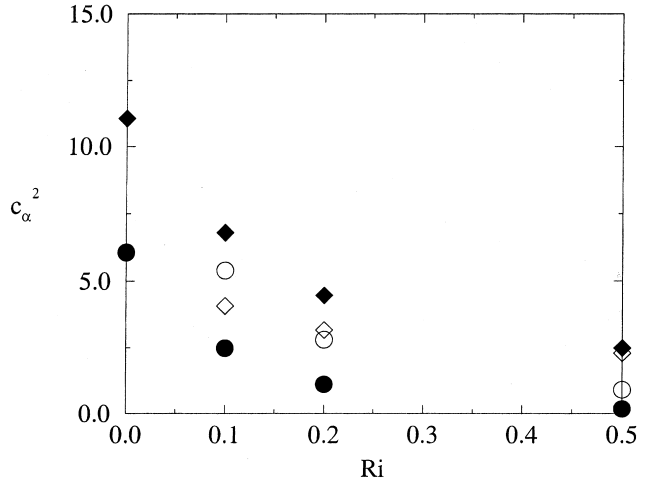

Fig. 8. Dependence of the square of the concentration fluctuations c_2^2 and c_3^2 on the Richardson number Ri for the vertical shear case (filled symbols) and the horizontal shear case (open symbols) at nondimensional time $St = 10$. Circles correspond to c_3^2 and diamonds correspond to c_2^2.

3.3. Turbulent mixing

Turbulent mixing of momentum and mass can be studied by consideration of the eddy viscosity ν_t of the velocity field and the eddy diffusivity α_t of the concentration fields. In the vertical shear case, the vertical velocity gradient results in a turbulent momentum transport in the vertical direction. In the horizontal shear case, the horizontal velocity gradient results in a turbulent momentum transport in the horizontal direction:

$$\nu_t^V = -\frac{\overline{u_1 u_3}}{S_V}, \qquad \nu_t^H = -\frac{\overline{u_1 u_2}}{S_H}. \tag{14}$$

The concentration fields have vertical as well as horizontal gradients. Therefore, turbulent mass transport in the vertical and horizontal directions can be considered

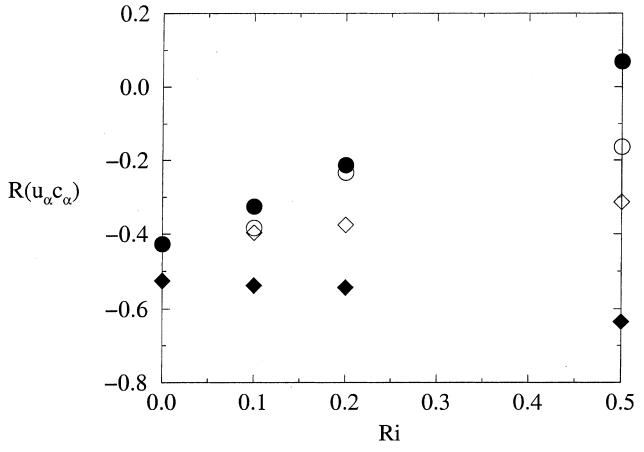

Fig. 9. Dependence of the correlation coefficients $R(u_3c_3)$ and $R(u_2c_2)$ on the Richardson number Ri for the vertical shear case (filled symbols) and the horizontal shear case (open symbols) at nondimensional time $St = 10$. Circles correspond to $R(u_3c_3)$ and diamonds correspond to $R(u_2c_2)$.

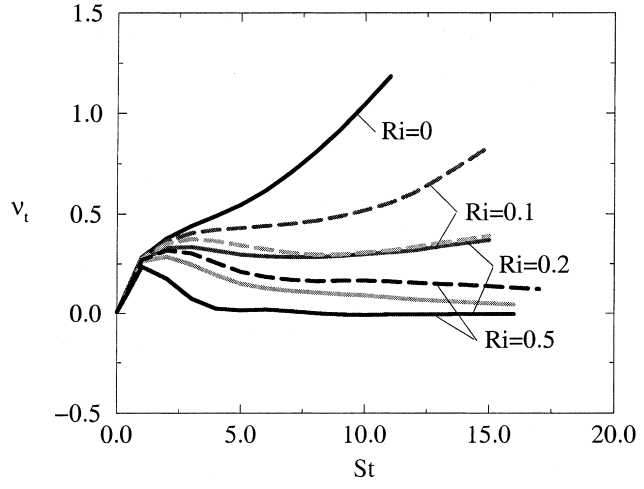

Fig. 10. Evolution of the eddy viscosity ν_t as a function of the Richardson number Ri for the vertical shear case (solid lines) and the horizontal shear case (dashed lines).

$$\alpha_t^V = -\frac{\overline{u_3 c_3}}{H_3}, \qquad \alpha_t^H = -\frac{\overline{u_2 c_2}}{H_2}. \tag{15}$$

In the following, the eddy viscosity ν_t and the eddy diffusivity α_t are computed from the direct numerical data.

Fig. 10 shows the evolution of the eddy viscosity ν_t as a function of the Richardson number Ri for the vertical and horizontal shear cases. As the Richardson number is increased, the eddy viscosity ν_t is decreased. However, for a given Richardson number Ri, the eddy viscosity ν_t^H of the horizontal shear case is always larger than the eddy viscosity ν_t^V of the vertical shear case.

In order to compare the effect of turbulence on the mixing of momentum and mass, the turbulent Schmidt number Sc_t is considered. In the vertical shear case, the turbulent Schmidt number is defined as the ratio of the turbulent diffusivities of momentum and mass in the vertical direction. In the horizontal shear case, the turbulent Schmidt number is defined as

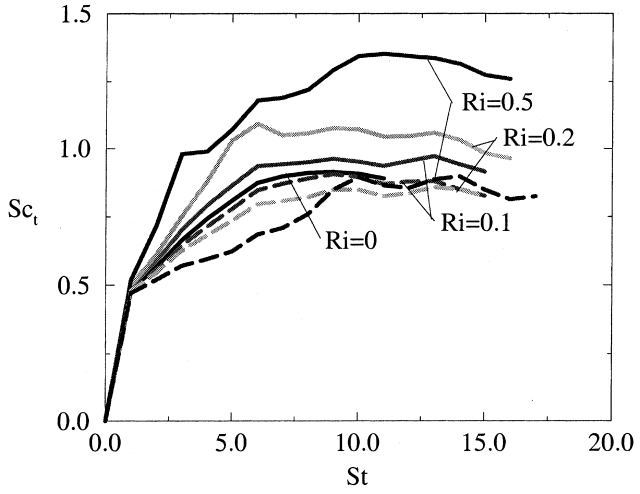

Fig. 11. Evolution of the turbulent Schmidt number Sc_t as a function of the Richardson number Ri for the vertical shear case (solid lines) and the horizontal shear case (dashed lines).

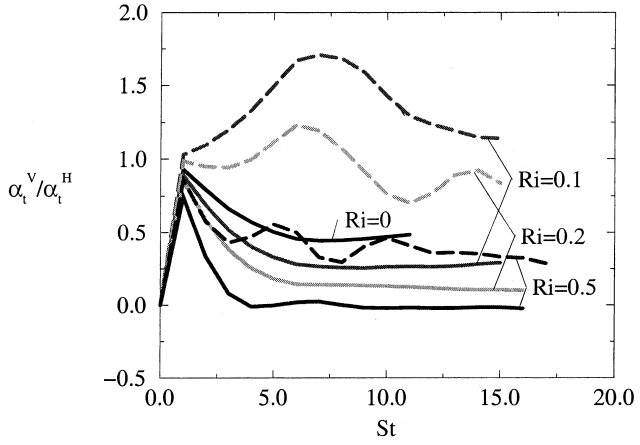

Fig. 12. Evolution of the ratio of vertical eddy diffusivity to horizontal eddy diffusivity α_t^V/α_t^H as a function of the Richardson number Ri for the vertical shear case (solid lines) and the horizontal shear case (dashed lines).

the ratio of the turbulent diffusivities of momentum and mass in the horizontal direction

$$Sc_t^V = \nu_t^V/\alpha_t^V, \qquad Sc_t^H = \nu_t^H/\alpha_t^H. \tag{16}$$

The evolution of the turbulent Schmidt number Sc_t as a function of the Richardson number Ri is shown in Fig. 11. In the vertical shear case, the turbulent Schmidt number Sc_t^V increases as the Richardson number is increased. This is consistent with the results of Schumann and Gerz (1995). In the horizontal shear case, however, the turbulent Schmidt number, remains constant and close to the value of the molecular Schmidt number $Sc = 0.72$ for all Richardson numbers.

Fig. 12 shows the evolution of the ratio of the vertical eddy diffusivity to the horizontal diffusivity α_t^V/α_t^H. In the vertical and horizontal shear cases, the ratio α_t^V/α_t^H decreases as the Richardson number Ri is increased. Here, the increasing density stratification inhibits vertical transport. The ratio α_t^V/α_t^H is always larger in the horizontal shear case compared to the vertical shear case for a given Richardson number. In the $Ri = 0.1$ case with horizontal the ratio is larger than 1.

4. Summary

Turbulent stratified shear flow has been studied using direct numerical simulations. Two series of simulations have been performed. The first series has vertical shear and the second series has horizontal shear. Both series are vertically stably stratified. It was found that the growth of the turbulent kinetic energy weakens as the Richardson number is increased. However, for the same value of the Richardson number, the horizontal shear case shows a stronger growth of the turbulent kinetic energy than the vertical shear case.

The turbulent kinetic energy is unevenly distributed over the velocity components. In the vertical shear case, the velocity components are ordered *streamwise* > *horizontal* > *vertical*. However, in the horizontal shear case, the order is changed to *streamwise* > *vertical* > *horizontal*. The change in the ordering of the horizontal and vertical velocity components can be explained by an increased pressure–strain redistribution of energy into the vertical velocity component in the horizontal shear case.

In addition, the evolution of concentration fields with mean gradients in the horizontal and vertical direction was studied. It was found that the concentration fluctuation of the species with the horizontal gradient is generally larger than the concentration fluctuation of the species with the vertical gradient. Only the low Richardson number case with horizontal shear shows the opposite result. This result is in contrast to the finding that the vertical velocity fluctuation is larger that the horizontal velocity fluctuation in the horizontal shear case. However, it can be explained with a decrease of the vertical correlation coefficient $R(u_3c_3)$ that controls the generation of vertical concentration fluctuations.

Finally, the turbulent transport properties of momentum and mass were compared. It was found that the turbulent eddy viscosities and diffusivities decrease as the Richardson number is increased. However, the eddy viscosity is always larger in the horizontal shear case compared to the vertical shear case for a given Richardson number. Also, the ratio of vertical eddy diffusivity to horizontal eddy diffusivity is always larger in the horizontal shear case for a given Richardson number.

References

Armi, L., 1978. Some evidence for boundary mixing in the deep ocean. J. Geophys. Res. 83, 1971–1979.

Caldwell, D.R., 1987. Small-scale physics of the ocean. Rev. Geophys. 25, 183–192.

Caldwell, D.R., Moum, J.N., 1995. Turbulence and mixing in the ocean. Rev. Geophys. 33, 1385–1394.

Farmer, D.M., D'Asaro, E.A., Trevorrow, M.V., Dairiki, G.T., 1995. Three-dimensional structure in a tidal convergence front. Cont. Shelf Res. 15, 1649–1673.

Foreman, M., Walters, R.A., Henry, R.F., 1993. A model for simulating currents in the eastern Juan de Fuca and the southern Strait of Georgia. In: Proceedings of the IEEE OCEANS 93, vol. 1, pp. 335–340.

Gerz, T., Schumann, U., Elghobashi, S.E., 1989. Direct numerical simulation of stratified homogeneous turbulent shear flows. J. Fluid Mech. 200, 563–594.

Gregg, M.C., 1987. Diapycnal mixing in the thermocline: A review. J. Geophys. Res. 92, 5249–5286.

Holt, S.E., Koseff, J.R., Ferziger, J.H., 1992. A numerical study of the evolution and structure of homogeneous stably stratified sheared turbulence. J. Fluid Mech. 237, 499–539.

Jacobitz, F.G., Sarkar, S., Atta, C.W., 1997. Direct numerical simulations of the turbulence evolution in a uniformly sheared and stably stratified flow. J. Fluid Mech. 342, 231–261.

Jacobitz, F.G., Sarkar, S., 1998. The effect of nonvertical shear on turbulence in a stably stratified medium. Phys. Fluids 10, 1158–1168.

Kaltenbach, H.-J., Gerz, T., Schumann, U., 1994. Large-eddy simulation of homogeneous turbulence and diffusion in stably stratified shear flow. J. Fluid Mech. 280, 1–40.

Lesieur, M.. Turbulence in Fluids, Kluver Academic Publishers, Dordrecht.

Lueck, R.G., Mudge, T.D., 1997. Topographically induced mixing around a shallow seamount. Science 276, 1831–1833.

Munk, W.H., 1966. Abyssal recipes. Deep Sea Res. 13, 707–730.

Piccirillo, P.S., Atta, C.W., 1997. The evolution of a uniformly sheared thermally stratified turbulent flow. J. Fluid Mech. 334, 61–86.

Rohr, J.J., Itsweire, E.C., Helland, K.N., Atta, C.W., 1988. Growth and decay of turbulence in a stably stratified shear flow. J. Fluid Mech. 195, 77–111.

Schumann, U., Gerz, T., 1995. Turbulent mixing in stably stratified shear flows. L. Appl. Meteorol. 34, 33–48.